The Astrophysical Journal Letters, 977:L5 (10pp), 2024 December 10 https://doi.org/10.3847/2041-8213/ad927c
© 2024. The Author(s). Published by the American Astronomical Society.
OPEN ACCESS

Three Quenched, Faint Dwarf Galaxies in the Direction of NGC 300: New Probes of Reionization and Internal Feedback

David J. Sand[1], Burçin Mutlu-Pakdil[2], Michael G. Jones[1], Ananthan Karunakaran[3], Jennifer E. Andrews[4], Paul Bennet[5], Denija Crnojević[6], Giuseppe Donatiello[7], Alex Drlica-Wagner[8,9,10], Catherine Fielder[1], David Martínez-Delgado[11,12], Clara E. Martínez-Vázquez[4], Kristine Spekkens[13], Amandine Doliva-Dolinsky[2,6], Laura C. Hunter[2], Jeffrey L. Carlin[14], William Cerny[15], Tehreem N. Hai[16], Kristen B.W. McQuinn[5,16], Andrew B. Pace[17], and Adam Smercina[5,18]

[1] Steward Observatory, University of Arizona, 933 North Cherry Avenue, Tucson, AZ 85721-0065, USA; dsand@arizona.edu
[2] Department of Physics and Astronomy, Dartmouth College, 6127 Wilder Laboratory, Hanover, NH 03755, USA
[3] Department of Astronomy & Astrophysics, University of Toronto, Toronto, ON M5S 3H4, Canada
[4] International Gemini Observatory/NSF NOIRLab, 670 N. A'ohoku Place, Hilo, HI 96720, USA
[5] Space Telescope Science Institute, 3700 San Martin Drive, Baltimore, MD 21218, USA
[6] Department of Physics & Astronomy, University of Tampa, 401 West Kennedy Boulevard, Tampa, FL 33606, USA
[7] Unione Astrofili Italiani P.I. Sezione Nazionale di Ricerca Profondo Cielo, 72024 Oria, Italy
[8] Fermi National Accelerator Laboratory, P.O. Box 500, Batavia, IL 60510, USA
[9] Kavli Institute for Cosmological Physics, University of Chicago, Chicago, IL 60637, USA
[10] Department of Astronomy and Astrophysics, University of Chicago, Chicago, IL 60637, USA
[11] Centro de Estudios de Física del Cosmos de Aragón (CEFCA), Unidad Asociada al CSIC, Plaza San Juan 1, 44001 Teruel, Spain
[12] ARAID Foundation, Avda. de Ranillas, 1-D, E-50018 Zaragoza, Spain
[13] Department of Physics, Engineering Physics and Astronomy, Queen's University, Kingston, ON K7L 3N6, Canada
[14] AURA/Rubin Observatory, 950 North Cherry Avenue, Tucson, AZ 85719, USA
[15] Department of Astronomy, Yale University, New Haven, CT 06520, USA
[16] Department of Physics and Astronomy, Rutgers, the State University of New Jersey, 136 Frelinghuysen Road, Piscataway, NJ 08854, USA
[17] Department of Astronomy, University of Virginia, 530 McCormick Road, Charlottesville, VA 22904, USA
Received 2024 September 20; revised 2024 November 11; accepted 2024 November 13; published 2024 December 2

Abstract

We report the discovery of three faint and ultrafaint dwarf galaxies—Sculptor A, Sculptor B, and Sculptor C—in the direction of NGC 300 ($D = 2.0$ Mpc), a Large Magellanic Cloud–mass galaxy. Deep ground-based imaging with Gemini/GMOS resolves all three dwarf galaxies into stars, each displaying a red giant branch indicative of an old, metal-poor stellar population. No young stars or H I gas are apparent, and the lack of a GALEX UV detection suggests that all three systems are quenched. Sculptor C ($D = 2.04^{+0.10}_{-0.13}$ Mpc; $M_V = -9.1 \pm 0.1$ mag or $L_V = (3.7^{+0.4}_{-0.3}) \times 10^5 L_\odot$) is consistent with being a satellite of NGC 300. Sculptor A ($D = 1.35^{+0.22}_{-0.08}$ Mpc; $M_V = -6.9 \pm 0.3$ mag or $L_V = (5^{+1}_{-1}) \times 10^4 L_\odot$) is likely in the foreground of NGC 300 and at the extreme edge of the Local Group, analogous to the recently discovered ultrafaint Tucana B in terms of its physical properties and environment. Sculptor B ($D = 2.48^{+0.21}_{-0.24}$ Mpc; $M_V = -8.1 \pm 0.3$ mag or $L_V = (1.5^{+0.5}_{-0.4}) \times 10^5 L_\odot$) is likely in the background, but future distance measurements are necessary to solidify this statement. It is also of interest due to its quiescent state and low stellar mass. Both Sculptor A and B are $\gtrsim$2–4 $r_{\rm vir}$ from NGC 300 itself. The discovery of three dwarf galaxies in isolated or low-density environments offers an opportunity to study the varying effects of ram-pressure stripping, reionization, and internal feedback in influencing the star formation history of the faintest stellar systems.

Unified Astronomy Thesaurus concepts: Dwarf galaxies (416); Quenched galaxies (2016); Galaxy quenching (2040)

1. Introduction

The faintest galaxies are essential proving grounds for understanding dark matter and astrophysics on small scales (J. S. Bullock & M. Boylan-Kolchin 2017; J. D. Simon 2019; L. V. Sales et al. 2022 for recent reviews). A hallmark of the Lambda Cold Dark Matter model is that structure forms hierarchically: galaxies inhabit dark matter halos, which contain dark matter substructures that often host smaller galaxies. Understanding this hierarchical structure formation in detail at subgalactic scales has led to continuing, intensive efforts to observe and quantify the satellite system of the Milky Way (e.g., A. Drlica-Wagner et al. 2020; W. Cerny et al. 2023; S. E. T. Smith et al. 2023, 2024; M. Gatto et al. 2024; D. Homma et al. 2024), M31 (e.g., N. F. Martin et al. 2013; A. Doliva-Dolinsky et al. 2022, 2023), and other nearby Milky Way–like galaxies (e.g., K. Chiboucas et al. 2013; D. Crnojević et al. 2016b, 2019; A. Smercina et al. 2018; P. Bennet et al. 2019, 2020; S. G. Carlsten et al. 2022; Y.-Y. Mao et al. 2021, 2024; B. Mutlu-Pakdil et al. 2024). Meanwhile, numerical simulations that include baryonic astrophysics have made significant progress in reproducing the dwarf galaxy properties of bright systems observed in Milky Way–mass systems (e.g., A. M. Brooks et al. 2013; T. Sawala et al. 2016; A. R. Wetzel et al. 2016; J. Samuel et al. 2021; C. Engler et al. 2021), while semianalytic models are successful for fainter systems (e.g., V. Manwadkar & A. V. Kravtsov 2022; S. Weerasooriya et al. 2023; N. Ahvazi et al. 2024).

[18] Hubble Fellow.

Original content from this work may be used under the terms of the Creative Commons Attribution 4.0 licence. Any further distribution of this work must maintain attribution to the author(s) and the title of the work, journal citation and DOI.

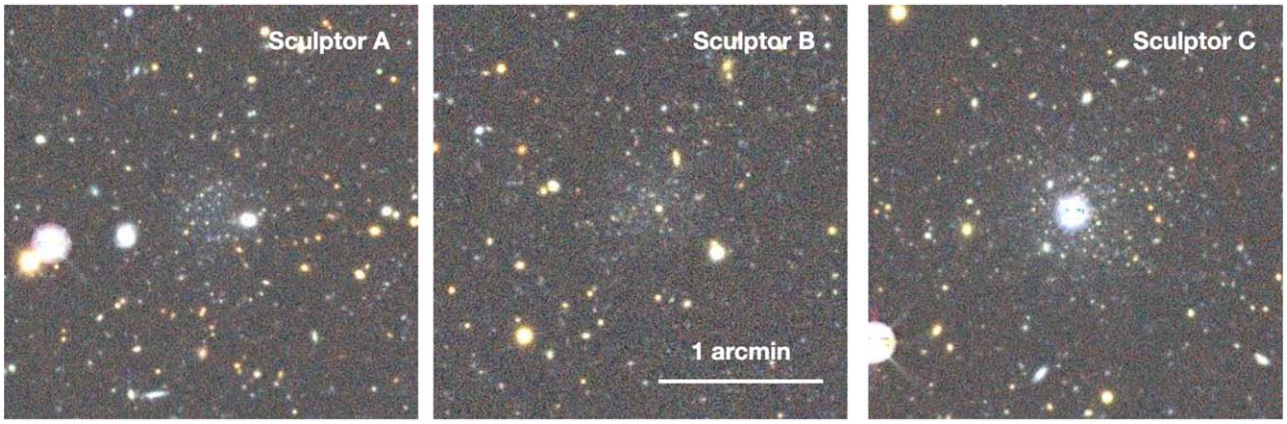

Figure 1. Sculptor A, B, and C as seen in the DESI Legacy Imaging Surveys sky browser. North is up, and east is to the left. Note the bright foreground star projected onto Sculptor C.

To complement and extend observations around Milky Way–mass systems and to test the astrophysics input into modern simulations, it is necessary to identify and understand the lowest-mass dwarf galaxies in a variety of environments. One area of interest is the population of dwarfs in lower-density environments: at the edge of the Local Group's main galaxies (e.g., K. B. W. McQuinn et al. 2023, 2024), around less massive hosts such as Magellanic Cloud–like systems (e.g., D. J. Sand et al. 2015a; J. L. Carlin et al. 2016; J. L. Carlin et al. 2021, 2024; A. B. Davis et al. 2024; M. McNanna et al. 2024) and in isolation (e.g., J. M. Cannon et al. 2011; K. B. W. McQuinn et al. 2014, 2021; D. J. Sand et al. 2022; M. G. Jones et al. 2023, 2024; J. Li et al. 2024). The effects of tidal and ram-pressure stripping will be diminished in low-density environments (e.g., C. T. Garling et al. 2024), with the exception of "backsplash" systems (e.g., M. Teyssier et al. 2012; T. Buck et al. 2019; I. M. E. Santos-Santos et al. 2023), and so offer an opportunity to cleanly study other quenching mechanisms, such as reionization (J. S. Bullock et al. 2000; A. J. Benson et al. 2002; M. Ricotti & N. Y. Gnedin 2005; M. Jeon et al. 2017; E. Applebaum et al. 2021) and star formation/supernova feedback (e.g., A. Dekel & J. Silk 1986; M.-M. Mac Low & A. Ferrara 1999; P. F. Hopkins et al. 2012; K. El-Badry et al. 2018).

Here, we report the discovery of three faint, seemingly quenched, dwarf galaxies in the direction of NGC 300. NGC 300 is an SA spiral galaxy at $D = 2.0$ Mpc (based on the tip of the red giant branch, TRGB; J. J. Dalcanton et al. 2009) in the direction of the Sculptor group. It has a K-band luminosity very similar to the Large Magellanic Cloud (LMC; B. Mutlu-Pakdil et al. 2021), making it an excellent comparison for satellite population studies.[18] Throughout this work, we assume that NGC 300 has a virial radius of $r_{\rm vir} \approx 120$ kpc and halo mass of $\log(M_{\rm halo}/M_{\odot}) \approx 11.29$ as calculated in B. Mutlu-Pakdil et al. (2021), using the stellar mass–halo mass relation of B. P. Moster et al. (2010). These values are uncertain but are used to help ascertain the relationship between the three faint dwarf discoveries and NGC 300, with this caveat in mind. We present the discovery of the three dwarf galaxies in Section 2 and discuss follow-up optical observations in Section 3. In Section 4, we measure the basic physical properties of the dwarfs (distance, stellar population, gas content, structure, and luminosity). We discuss the environment of each in Section 5 and compare them with other dwarfs in low-density environments. Finally, we summarize and conclude in Section 6.

2. Ultrafaint Dwarf Galaxy Discovery around NGC 300

Following the recent discovery of Tucana B through a focused visual search utilizing the DESI Legacy Imaging Surveys and its interactive color image viewer[19](D. J. Sand et al. 2022), we began a systematic search for faint companions around other nearby galaxies ($D \lesssim 2$ Mpc), including NGC 300 (for reference, Data Release, DR, 9 of the DESI Legacy Imaging Surveys was used). We uploaded a custom file to mark off a region with a projected box size of 400 kpc on a side centered on NGC 300 itself ($\approx$11.3°) and visually searched for stellar overdensities with underlying diffuse light. This coverage area out to $R_{\rm proj} \sim 200$ kpc encloses the full virial radius of NGC 300, which is approximately 120 kpc (B. Mutlu-Pakdil et al. 2021). Faint dwarf galaxies at the distance of NGC 300 can resemble "semiresolved" objects, with both resolved and diffuse components, at the depth of DECaLS (g, $r \approx$ 23.5–24 mag, depending on the field; A. Dey et al. 2019). We searched the NGC 300 footprint several times, at different spatial scales and contrast levels.

Three high-confidence faint dwarf galaxy candidates stood out during the search, and we show color cutouts obtained from the Legacy Survey Image Viewer in Figure 1. We also present a schematic of the footprint searched and the projected position of these discoveries in Figure 2. NGC 300 and surrounding areas are in the footprint of the Dark Energy Survey (DES; T. M. C. Abbott et al. 2021) DR2, and we downloaded photometry of the field using NOIRLab's Query Interface Tool.[20] This photometry was suggestive of an old, metal-poor red giant branch (RGB) at $\sim$2 Mpc but was ultimately inconclusive. We thus sought deeper ground-based optical imaging, which we discuss next.

We choose the names Sculptor A, Sculptor B, and Sculptor C for the three new faint dwarfs because of the constellation they reside in and the fact that we are uncertain if each of these dwarfs is associated with NGC 300 (as we address in later

[18] If we use a K-band mass-to-light ratio of 1, both NGC 300 and the LMC have a stellar mass of $\sim 2.6 \times 10^9\ M_{\odot}$. This is consistent with stellar mass estimates of $2 \times 10^9\ M_{\odot}$ for NGC 300 (J. C. Muñoz et al. 2015) and $2.7 \times 10^9\ M_{\odot}$ for the LMC (R. P. van der Marel et al. 2002) in the literature.

[19] https://www.legacysurvey.org/viewer

[20] https://datalab.noirlab.edu/query.php

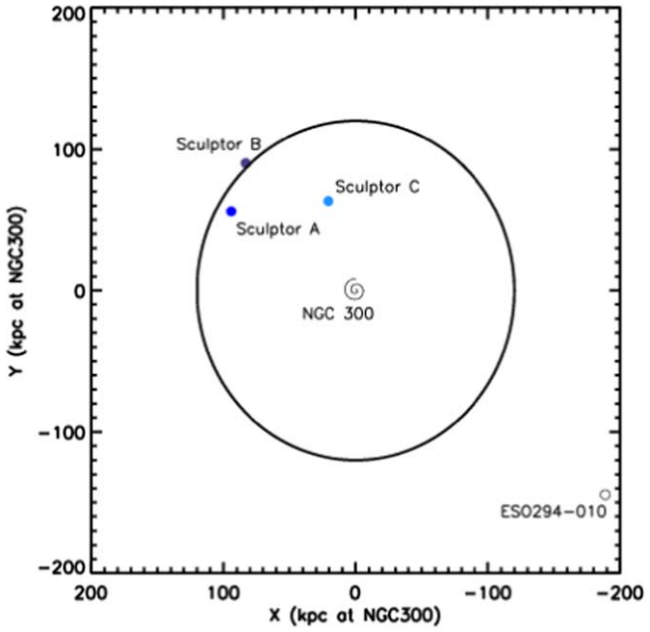

Figure 2. Spatial footprint of our visual search for dwarfs associated with NGC 300. The solid line marks the approximate projected virial radius at $R_{\rm vir,NGC300} = 120$ kpc (B. Mutlu-Pakdil et al. 2021), and the unfilled point shows the position of ESO294-010 ($D = 1.94$ Mpc; $M_{\rm B} = -10.9$ mag; J. J. Dalcanton et al. 2009), a previously known dwarf galaxy that may be associated with NGC 300. To our knowledge, these are the only known galaxies within the virial region of NGC 300 although the galaxy NGC 55 (also at $D = 2$ Mpc) is directly to the west of this field. The spatial position of Sculptors A, B, and C are shown. Sculptor A ($D = 1.35^{+0.22}_{-0.08}$ Mpc) and Sculptor B ($D = 2.48^{+0.21}_{-0.24}$ Mpc) are both at the approximate virial radius of NGC 300 in projection and are ∼500 kpc offset in distance as well. We discuss the membership status of the identified dwarfs further in Section 5.1.

sections of this Letter). A similar naming convention has been used for other dwarfs just beyond the edge of the Local Group.

3. Gemini Deep Optical Follow-Up

After the visual discovery of Sculptor A, B, and C, we obtained deep follow-up imaging of all three systems with the Gemini South telescope using the Gemini Multi-Object Spectrograph (GMOS; I. M. Hook et al. 2004) under the Fast Turnaround program GS-2022B-FT-103. The GMOS images have a ≈5.′5 × 5.′5 field of view and 0.″16 pixel^{-1} scale after binning. Both g- and r-band imaging was taken for all three dwarfs, with strict image quality constraints, between 2022 August 29 and 2022 September 30 (UT). For Sculptors A and B, we took 7 × 300 s exposures in both bands. For Sculptor C, we obtained 16 × 120 s exposures in both bands in order to mitigate the effects of the bright foreground star centered on the dwarf (see Figure 1). Small dithers were taken between exposures. At the time of the observations, GMOS South suffered from a bad amplifier, which we were careful to avoid in our observational setup. All data associated with this amplifier were masked during the data reduction process.

Initial data reduction for the Gemini data was done with DRAGONS (K. Labrie et al. 2023a), the pipeline maintained by Gemini Observatory. DRAGONS performs bias subtraction, flat-field correction, and bad pixel masking on the images. Cosmic rays were rejected using the sigma-clipping method within the DRAGONS pipeline. Stacked images were created using the weighted average of the constituent images. As a final step, an astrometric correction was applied by using SCAMP (E. Bertin 2006). The final g- and r- band stacked images had point-spread function FWHM values between 0.″6 and 0.″8.

We performed point-spread function fitting photometry on the stacked GMOS images, using DAOPHOT and ALLFRAME (P. B. Stetson 1987, 1994), following the general procedure described in B. Mutlu-Pakdil et al. (2018). The photometry was calibrated to point sources in the DES DR2 catalog (T. M. C. Abbott et al. 2021), including a color term, and was corrected for Galactic extinction (E. F. Schlafly & D. P. Finkbeiner 2011) on a star-by-star basis. The typical color excess at the position of the dwarfs is $E(B - V) = 0.014$–0.015 mag (see Table 1). In the remainder of this work, we present dereddened g_0 and r_0 magnitudes, unless otherwise stated.

To determine our photometric errors and completeness as a function of magnitude and color, we conduct artificial star tests with the DAOPHOT routine ADDSTAR, similar to previous work (B. Mutlu-Pakdil et al. 2018). Over several iterations, we injected ∼10^5 artificial stars into our stacked images with a range of magnitudes ($r = 18$–29 mag) and colors ($g - r = -0.5$ to 1.5) and then photometered the simulated data in the same way as the original images. The 50% (90%) completeness level was at $r = 26.4$, 26.3, 26.4 (25.4, 25.1, 25.5) and $g = 26.7$, 26.7, 27.0 (25.5, 25.5, 25.9) mag for Sculptor A, B, and C, respectively.

In Figure 3, we show the color–magnitude diagrams (CMDs) of our three dwarfs within their half-light radius, r_h, as derived in Section 4.3. As can be seen, each dwarf has a clear but sparsely populated RGB whose brightest stars are at different magnitudes from dwarf to dwarf, likely indicating that these systems are at different distances. We discuss the structure and stellar populations of these new dwarfs in Section 4.

4. Dwarf Galaxy Physical Properties

In this section, we measure the physical properties of the three newly discovered dwarf galaxies, using the deep Gemini photometry, as well as archival H I and Galaxy Evolution Explorer (GALEX) UV data sets. The properties we derive are shown in Table 1.

4.1. Distance

As we will discuss in Section 4.2, the stellar populations of all three dwarf galaxies exhibit sparsely populated, old, metal-poor RGBs, with no other stellar population apparent (see Figure 3). Because of this sparse population, with few stars populating the brightest regions of the RGB, only one of the three dwarfs displays a clear TRGB, which could be used for measuring a distance (Sculptor C; see below). The Gemini data are also not deep enough to obtain a distance based on the horizontal branch or RR Lyrae stars although the first signs of a horizontal branch may be visible in Sculptor A at the faintest magnitudes, as we discuss below.

For consistency, we thus measure the distance to the three dwarf galaxies using a CMD-fitting technique, comparing the number of stars consistent with an old, metal-poor theoretical isochrone as a function of assumed distance. A similar technique has been used to measure the distance to many Milky Way ultrafaint dwarf galaxies (e.g., S. M. Walsh et al. 2008; D. J. Sand et al. 2009), as well as Tucana B (D. J. Sand et al. 2022). In our analysis, we use Dartmouth isochrones (A. Dotter et al. 2008) with a 13.5 Gyr stellar population and low metallicities ([Fe/H] = −2.5, −2.0, and −1.5.). For each

Table 1
Faint Dwarf Galaxy Properties

Parameter	Sculptor A	Sculptor B	Sculptor C
α_0 (J2000)	01:08:30.8 ± 2.″4	01:06:50.9 ± 3.″6	00:57:52.2 ± 3.″1
δ_0 (J2000)	−36:03:52.9 ± 3.″2	−35:04:39.0 ± 2.″7	−35:51:08.4 ± 4.″0
$E(B-V)$ (mag)	0.015	0.015	0.014
$m-M$ (mag)	$25.65^{+0.33}_{-0.13}$	$26.98^{+0.17}_{-0.23}$	$26.55^{+0.10}_{-0.13}$
Distance (Mpc)	$1.35^{+0.22}_{-0.08}$	$2.48^{+0.21}_{-0.24}$	$2.04^{+0.10}_{-0.11}$
$R_{\rm proj,NGC300}$ (kpc)[a]	109	123	67
$D_{\rm 3D,NGC300}$ (kpc)[b]	660^{+80}_{-220}	500^{+210}_{-230}	80^{+80}_{-13}
M_V (mag)	−6.9 ± 0.3	−8.1 ± 0.3	−9.1 ± 0.1
L_V ($L_\odot$)	$(5^{+1}_{-1})\times10^4$	$(1.5^{+0.5}_{-0.4})\times10^5$	$(3.7^{+0.4}_{-0.3})\times10^5$
$\log(M_*/M_\odot)$	4.7 ± 0.1	5.1 ± 0.1	5.7 ± 0.1
r_h (arcsec)	16.8 ± 4.2	20.4 ± 7.1	36.6 ± 4.2
r_h (pc)	110 ± 28	245 ± 85	362 ± 42
ϵ	0.34 ± 0.17	0.41 ± 0.22	0.24 ± 0.10
θ (deg)	−11.5 ± 17.5	133.1 ± 29.2	66.9 ± 12.6
$\log(\mathrm{SFR_{NUV}}/M_\odot\ \mathrm{yr}^{-1})$	<6.0	<5.3	<4.8
$\log(\mathrm{SFR_{FUV}}/M_\odot\ \mathrm{yr}^{-1})$	<6.3	<5.6	<6.0
$\log(M_{\rm HI}/M_\odot)$	<5.3	<5.8	<5.6

Notes.
[a] Projected radius with respect to NGC 300 ($D=2$ Mpc).
[b] 3D distance between dwarf galaxy and NGC 300 ($D=2$ Mpc).

dwarf, we include all stars brighter than the 50% completeness threshold and stars spatially coincident with the main body of each dwarf (a radius of 0.′3–0.′5), assessed visually. Then, we shift each isochrone fiducial through distance moduli ($m-M$) between 25.0 and 28.0 mag (1.0 and 4.0 Mpc) in 0.025 mag steps, counting the number of stars consistent with the isochrone at that distance. A scaled background region at the edge of the GMOS field of view is used to subtract off contaminants for each distance modulus trial. For a given r_0, a star is considered consistent with the isochrone if its $(g-r)_0$ color is within a red/blue boundary derived from our photometric uncertainties. The best distance corresponds to the distance modulus that maximizes the number of stars consistent with the isochrone after background removal. To assess our uncertainties on the distance measurement, we bootstrap (resample with replacement) both the input dwarf stars and the background objects.

The fits to the $[\mathrm{Fe/H}]=-2.0$ isochrone are excellent, as are those for the $[\mathrm{Fe/H}]=-2.5$ isochrone, while the best-fitting $[\mathrm{Fe/H}]=-1.5$ isochrones are slightly too red and do not capture the shape of the observed RGB. For this reason, we adopt the $[\mathrm{Fe/H}]=-2.0$ distance in this work (see the second left panel in Figure 3), with the range of best-fitting distance values for the full metallicity set as our formal uncertainty. We choose this metric for the reported uncertainty rather than the results of the bootstrap analysis as the bootstrap uncertainties are subdominant in comparison to the distance spread between metallicities. We list these distances in Table 1.

As a check on our CMD-fitting results, we also found the distance to Sculptor C using a standard TRGB distance measurement technique. Here, we selected stars in the dwarf consistent with the RGB and measured the luminosity function of these stars, compared with a model luminosity function convolved with our photometric uncertainties and completeness as determined from our artificial star tests (see D. Crnojević et al. 2019 for further details). Using a nonlinear least-squares fit between model and data, we calculated a TRGB magnitude of $r_{\rm TRGB}=23.58\pm0.08$ mag. This results in a distance modulus of $m-M=26.59\pm0.13$ mag (assuming $M_r^{\rm TRGB}=-3.01\pm0.01$, which does not include systematic or zero-point uncertainties; D. J. Sand et al. 2014) and a distance of $D=2.08\pm0.12$ Mpc. This value is nearly identical to that determined through the CMD-fitting technique described above, so we stick with the original measurement for all three dwarfs, for consistency.

Interestingly, the distances to Sculptor A ($D=1.35^{+0.22}_{-0.08}$ Mpc) and Sculptor B ($D=2.48^{+0.21}_{-0.24}$ Mpc) are not clearly consistent with the distance to NGC 300 itself ($D=2.0$ Mpc), especially given that Sculptor A and Sculptor B are roughly at the projected virial radius of ≈120 kpc. We return to this and the membership status of the dwarfs in Section 5.1.

4.2. Stellar Population

The CMDs of all three dwarf galaxies appear to only consist of an old, metal-poor stellar population (Figure 3). Any younger blue stellar population either has few stars associated with it or is below our detection limit. Many of the recently discovered faint dwarf galaxies beyond the Local Group show distinct signs of recent star formation (e.g., Leo P, K. B. W. McQuinn et al. 2015; Antlia B, J. R. Hargis et al. 2020; Pavo, M. G. Jones et al. 2023) although a growing subset also appears to be quenched, with little to no recent star formation (e.g., Tucana B, D. J. Sand et al. 2022; Blobby, K. J. Casey et al. 2023; Hedgehog, J. Li et al. 2024). The mix of stellar populations of faint dwarf galaxies in the "field" is a critical ingredient for understanding the role of reionization, stellar feedback, and ram pressure from the cosmic web in driving the evolution of the smallest galaxies.

The distance to Sculptor A is near enough ($D=1.35$ Mpc) that we could plausibly have detected blue horizontal branch stars. Given the distance, such a population would reside at $r_0\approx26.3$ mag and $(g-r)_0\lesssim0$ mag. Visual inspection of the CMD in Figure 3 indicates that there may be an overdensity of

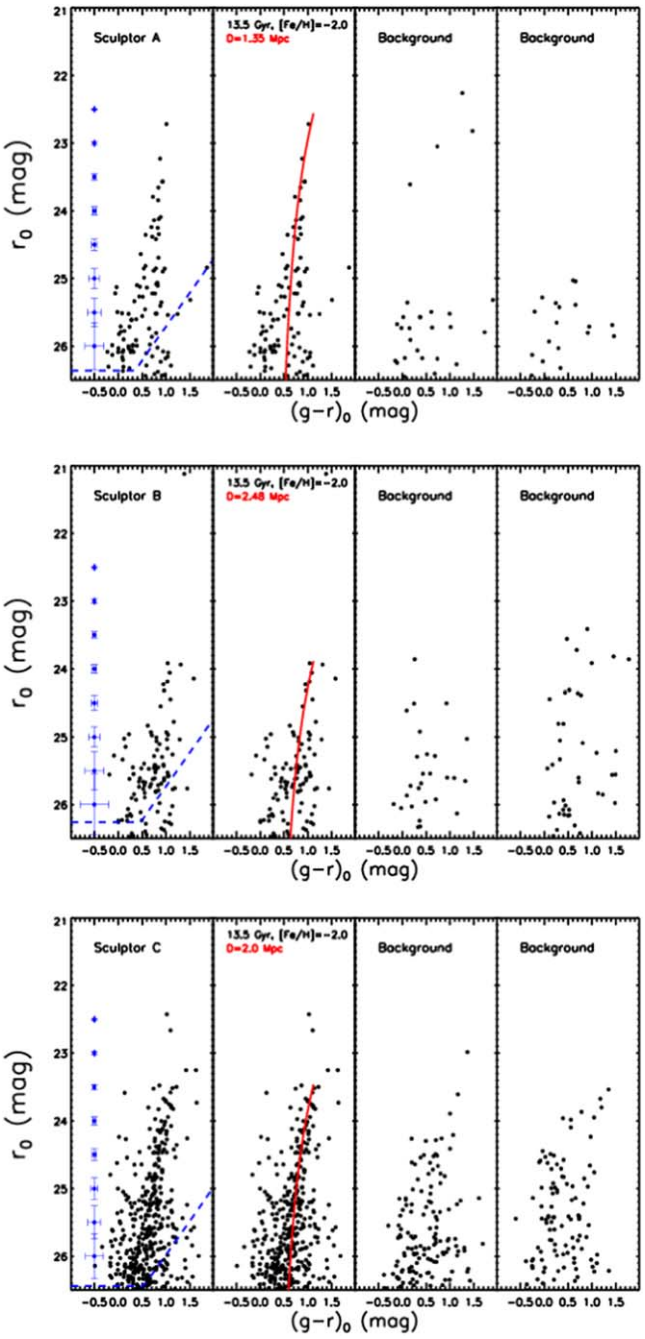

Figure 3. Deep CMDs for our three dwarf galaxies based on Gemini GMOS imaging data. For each plot, the left two panels display the CMD of the dwarf within 1.0 r_h (Section 4.3). Only point sources are plotted, as described in Section 3. The far left panel shows the typical uncertainties at different r-band magnitudes, while the dashed line marks the 50% completeness limit, both as determined by artificial star tests. The center left panel overplots a 13.5 Gyr, [Fe/H] = −2.0 isochrone (A. Dotter et al. 2008) at the distance determined by our CMD-fitting technique (Section 4.1). The two panels on the right show randomly selected background regions, chosen to be devoid of bright, saturated stars. The background regions have different areal coverage for each dwarf so that they are equivalent to that covered by the half-light radius.

stars in this region of color–magnitude space although the contamination is high and photometric uncertainties are significant. Space-based observations are necessary to confirm this population.

To constrain any possible young stellar population in each dwarf, we search for coincident UV emission with the GALEX (D. C. Martin et al. 2005) data archive. GALEX data from the All Sky Survey are available for Sculptor A and Sculptor B, while data from the Medium Imaging Survey are available for Sculptor C (see L. Bianchi et al. 2017 for details). GALEX observations are sensitive to star formation on $\lesssim$100 Myr timescales (J. C. Lee et al. 2011). For our measurements, we adopt the methodology of A. Karunakaran et al. (2021), using an aperture $1.33r_h$ in size (see Section 4.3) and placing down 1000 random apertures throughout the GALEX field to assess flux uncertainties (after masking bright objects). No flux was detected for any of the three dwarf galaxies, and we use the GALEX near-ultraviolet and far-ultraviolet flux limits to determine star formation rate limits using the relations of J. Iglesias-Páramo et al. (2006). See Table 1 for our 2σ star formation rate limits for each object. The star formation limits are $\log(\mathrm{SFR_{NUV}}/M_\odot\ \mathrm{yr}^{-1}) < -4.8$ and $\log(\mathrm{SFR_{FUV}}/M_\odot\ \mathrm{yr}^{-1}) < -5.6$ for all three dwarfs, which are more stringent than most UV detections in satellite galaxies around Milky Way–like galaxies (e.g., A. Karunakaran et al. 2021). While there is no recent star formation among the dwarfs, future space-based observations are necessary to characterize any faint, intermediate-age population ($\gtrsim$500 Myr; e.g., D. R. Weisz et al. 2014b).

4.3. Stellar Structure, Luminosity, and Stellar Mass

To measure the structural parameters of these sparse stellar systems, we fit an exponential profile to the two-dimensional distribution of stars consistent with the RGB in each system, using the maximum likelihood technique of N. F. Martin et al. (2008), as implemented in D. J. Sand et al. (2012). Stars throughout the GMOS field that are consistent with the best-fitting Dartmouth isochrone and distance are used in the analysis (see Section 4.1). The free parameters for the exponential fit are the central position (α_0, δ_0), position angle (θ), ellipticity ϵ, half-light radius (r_h), and a constant background surface density. Uncertainties are calculated using a bootstrap resampling analysis, with 1000 iterations. The maximum likelihood technique employed naturally accounts for portions of the image where point sources would be undetectable, such as the bad amplifier (mentioned in Section 3) and the bright star coincident with the main body of Sculptor C (see Figure 1). The results of the structural analysis are presented in Table 1. The dwarfs are ≈100–360 pc in size (as characterized by the half-light radius) and have moderate ellipticities ($\epsilon \approx 0.2$–0.4), which are all typical values for faint dwarf galaxies, as we will discuss in Section 5.

To measure the luminosity of the three dwarf galaxies, we employ the technique of N. F. Martin et al. (2008) in the "CMD shot noise" regime, when the presence or absence of individual stars in the upper regions of the RGB can significantly affect the overall luminosity. To do this, we produce a well-populated CMD using a 13.5 Gyr, [Fe/H] = −2 stellar population with a Salpeter initial mass function, convolving the stellar population with the photometric uncertainties and completeness derived from our artificial star tests. From this simulated CMD, we randomly draw the same number of stars as was found in our maximum likelihood analysis (which can account for missing areas of data such as the bright star in Sculptor C), and to this luminosity, we add the luminosity in the simulated population below our detection limit. We repeat this process 100 times, using the median and standard deviation as our final absolute

magnitude and uncertainty, including the distance uncertainty, into the final estimation. We convert to V-band magnitudes using the filter transformation of K. Jordi et al. (2006). Absolute magnitudes and luminosities in the V band are quoted in Table 1.

Finally, to estimate the stellar mass of each object, we use the $g - r$ color and magnitudes to determine the stellar-mass-to-light ratio using the T. Into & L. Portinari (2013) relation. The stellar masses closely track the V-band luminosity, as expected for old metal-poor stellar populations; see Table 1 for our derived values.

4.4. Gas Content

None of the three dwarfs are detected in H I line emission in the H I Parkes All Sky Survey (HIPASS; D. G. Barnes et al. 2001), suggesting that they are not gas rich. To determine upper limits on the H I masses of the dwarfs, we use the Galactic All Sky Survey (GASS; N. M. McClure-Griffiths et al. 2009; P. M. W. Kalberla et al. 2010; P. M. W. Kalberla & U. Haud 2015), which is more sensitive than HIPASS, but only has data within the velocity range $-500 < v/\mathrm{km\,s^{-1}} < 500$. Given the radial velocity of NGC 300 ($140\,\mathrm{km\,s^{-1}}$) and the distance estimates to the three dwarfs, this range is likely more than sufficient, but a caveat to our upper limits below is that they would not apply for $v > 500\,\mathrm{km\,s^{-1}}$. We also cannot be certain (without a prior velocity measurement) that H I line emission from the dwarfs is not hidden within MW emission.

We downloaded GASS spectral line cubes[21] for each dwarf and extracted a spectrum over 3×3 spatial pixels, centered on each target. We inspected these spectra (and the cubes) at spectral resolutions of 5 and $25\,\mathrm{km\,s^{-1}}$ but saw no significant emission features other than the MW and high-velocity clouds. We measured the rms noise at $25\,\mathrm{km\,s^{-1}}$ resolution for each dwarf, and assuming $25\,\mathrm{km\,s^{-1}}$ as a conservative fiducial velocity width, we estimated the 3σ upper limits in each case. These limits are given in Table 1. More stringent gas limits will be necessary to verify that these systems are truly gas free (down to $M_{\mathrm{H\,I}}/L_V \approx 1$; e.g., M. E. Putman et al. 2021).

5. Discussion

The three dwarf galaxies in this work are among the faintest quenched dwarfs discovered outside the Local Group. In this section, we discuss whether they are plausible satellites of NGC 300 and their environment more generally. From there, we compare the dwarfs to other systems in low-density environments outside the Local Group and Magellanic Cloud analogs.

5.1. Environment and NGC 300 Membership Status

The original goal of our visual search was to identify satellites of the LMC analog NGC 300. However, based on the measured distances and projected radii of our three new dwarfs, we must first assess whether they are likely satellites or foreground/background systems.

We plot the projected radial distribution of the three dwarfs with respect to NGC 300 in Figure 2, along with the only other known galaxy within the extended virial region of NGC 300, ESO294-010. First, two out of three of the dwarfs (Sculptor A and Sculptor B) are near the projected virial radius of NGC 300, with $R_{\mathrm{proj,NGC300}} = 109$ and 123 kpc, respectively. The third dwarf, Sculptor C, has a projected radius of $R_{\mathrm{proj,NGC300}} = 67$ kpc, and given it has a distance consistent with NGC 300 itself, we confidently assert that it is very likely to be a satellite.

Not only are Sculptors A and B in the projected outskirts of NGC 300, their distances also indicate that they may not be associated with the galaxy. At ≈1.35 Mpc, Sculptor A has a 3D distance of $D_{\mathrm{3D,NGC300}} = 660^{+80}_{-220}$ kpc, meaning it is at least $\gtrsim 3.7\,r_{\mathrm{vir,NGC300}}$ assuming a nominal $r_{\mathrm{vir,NGC300}} = 120$ kpc. Similarly, Sculptor B (at $D \approx 2.48$ Mpc) has a 3D distance from NGC 300 of $D_{\mathrm{3D,NGC300}} = 500^{+210}_{-230}$ kpc, or $\gtrsim 2.3\,r_{\mathrm{vir,NGC\,300}}$. Based on these distances, we suggest that both systems are not associated with NGC 300.

Despite the assessment that Sculptor B is not associated with NGC 300, several caveats are worth mentioning. First, it is still plausible that Sculptor B is a backsplash system of NGC 300, where the expectation is that such systems will be at $\lesssim 2.5\,r_{\mathrm{vir}}$ (M. Teyssier et al. 2012; B. Diemer & A. V. Kravtsov 2015; T. Buck et al. 2019; E. Applebaum et al. 2021). Recent work suggests that extreme backsplash systems at larger radii are possible; a future velocity measurement of Sculptor B will help distinguish between scenarios (see I. M. E. Santos-Santos et al. 2023 for a discussion of the Tucana dwarf). It is also true that little theoretical/numerical work on the backsplash systems of Magellanic Cloud–scale halos has been done. Such studies will be useful as near-future discoveries of faint dwarfs become more common. Finally, it is also the case that the virial radius of NGC 300 is not directly measurable and highly uncertain, making an assessment of Sculptor B's status even more difficult.

To investigate the environment of the new Sculptor dwarfs further, we plot their positions (along with other Local Volume dwarfs) on two projections of the supergalactic coordinate system in Figure 4. On the plot, we also highlight other recently discovered nearby dwarf galaxies in low-density and isolated environments. In this view, Sculptor A clearly appears in the foreground to NGC 300 and associated galaxies. The WLM galaxy is marginally closer to Sculptor A than NGC 300 (≈630 kpc) although they are consistent within the uncertainties. In this sense, Sculptor A is very similar to Tucana B, at a similar distance to the Milky Way and its nearest neighbor (IC 5152 at ≈620 kpc).

The LMC-mass galaxy NGC 55 ($D \approx 2$ Mpc) is a nearby neighbor to NGC 300, located to the west just outside the projected field of view of Figure 2. NGC 55 and NGC 300 are sometimes considered part of the same overall group of galaxies (e.g., A. W. McConnachie 2012). Interestingly, all three newly discovered Sculptor dwarfs are arrayed on one side of NGC 300 (in projection), in the direction opposite to that of NGC 55. Given the range of distances in the new Sculptor dwarfs, there is no evidence for planar structure although future refined distance measurements are necessary.

The quenched Sculptor dwarfs join a rapidly growing list of nearby, relatively isolated dwarf galaxy systems that span a range of star formation properties. They offer an opportunity to understand what drives star formation and quenching in systems far from a massive perturbing galaxy.

5.2. Comparisons with Dwarfs in Low-density Environments

We plot the size–luminosity relation of faint dwarf galaxies around the Milky Way in Figure 5, along with several other quenched dwarfs in isolated or low-density environments. These include the putative ultrafaint satellites of the LMC

[21] https://www.astro.uni-bonn.de/hisurvey/gass/index.php

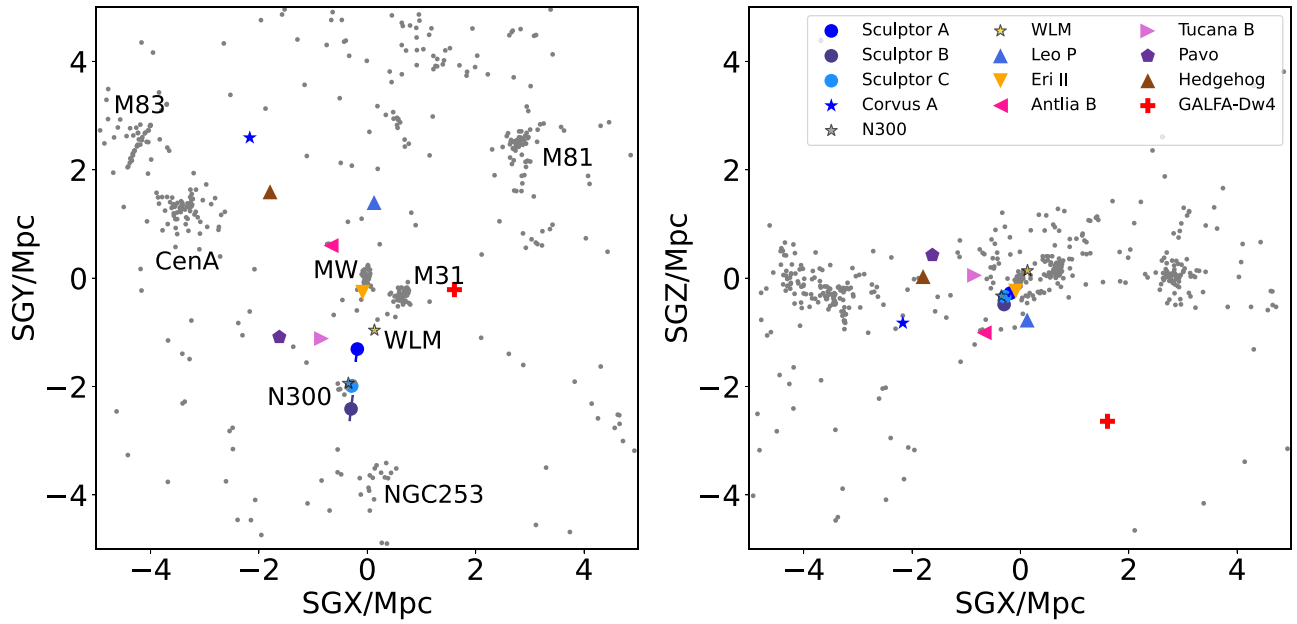

Figure 4. A map of nearby galaxies in supergalactic coordinates, illustrating the environment of Sculptors A, B, and C. Left: the supergalactic $X - Y$. Sculptors A, B, and C are shown, along with their appropriately scaled distance uncertainties. It is clear that Sculptor A and Sculptor B are in front of and behind NGC 300, respectively, in this projection. We show several other dwarfs in low density or isolated environments for reference: Corvus A (M. G. Jones et al. 2024); Leo P (R. Giovanelli et al. 2013); Eridanus II (D. Crnojević et al. 2016b); Antlia B (D. J. Sand et al. 2015a); GALFA-Dw4 (P. Bennet et al. 2022); Tucana B (D. J. Sand et al. 2022); Pavo (M. G. Jones et al. 2023); and Hedgehog (J. Li et al. 2024). Gray points are taken from the compilations of I. D. Karachentsev et al. (2004) and I. D. Karachentsev & E. I. Kaisina (2019). We also mark NGC 300 and the WLM galaxy, which are both mentioned in the text. Right: we show the supergalactic $X - Z$ plane and the local plane of galaxies.

(Reticulum II, Phoenix II, Horologium I, Hydrus I, Carina II, and Carina III; see, e.g., G. Battaglia et al. 2022), dwarfs associated with Magellanic Cloud analogs (MADCASH-1 and MADCASH-2; J. L. Carlin et al. 2021), several dwarfs at the edge of the Local Group (Tucana, Cetus, and Eridanus II), and even more isolated systems (Tucana B and Hedgehog). Overall, Sculptors A, B, and C are consistent with the size–luminosity relation of faint dwarfs in these various environments although surveys outside the Local Group do not have sensitivity to the ultrafaint dwarfs that are associated with the LMC.

Sculptor C ($M_V = -9.1$ mag; $r_h = 362$ pc) can be compared directly to recent faint dwarf galaxy discoveries around Magellanic Cloud analogs, given its very likely status as an NGC 300 satellite. Here MADCASH-2 ($M_V = -9.2$; $r_h = 130$ pc), associated with NGC 4214, is approximately the same luminosity but more compact. MADCASH-1 ($M_V = -7.8$; $r_h = 180$ pc; associated with NGC 2403) is a significantly fainter system (physical parameters for both dwarfs are from J. L. Carlin et al. 2021). Interestingly, Hubble Space Telescope data of MADCASH-2 show evidence for a small amount of recent star formation (<1.5 Gyr). Similar-quality data will be necessary to further investigate small amounts of recent star formation in our dwarf sample.

The known satellites of the Small Magellanic Cloud (SMC)–like galaxy NGC 3109 ($M_V \approx -15$, $D \approx 1.28$ Mpc; A. W. McConnachie 2012) offer another point of comparison. Both Antlia ($M_V = -10.4$) and Antlia B ($M_V = -9.4$ mag) have neutral gas reservoirs and notable recent star formation episodes (e.g., D. R. Weisz et al. 2011; D. J. Sand et al. 2015a; J. R. Hargis et al. 2020), in contrast to Sculptor C and the MADCASH dwarfs, although their greater masses may also contribute to their ability to retain gas in an SMC-like environment. Going forward, building a sample of satellite properties in the SMC-to-LMC-mass range may shed light on the effectiveness of ram-pressure stripping around lower-mass halos (see C. T. Garling et al. 2024 for a recent discussion).

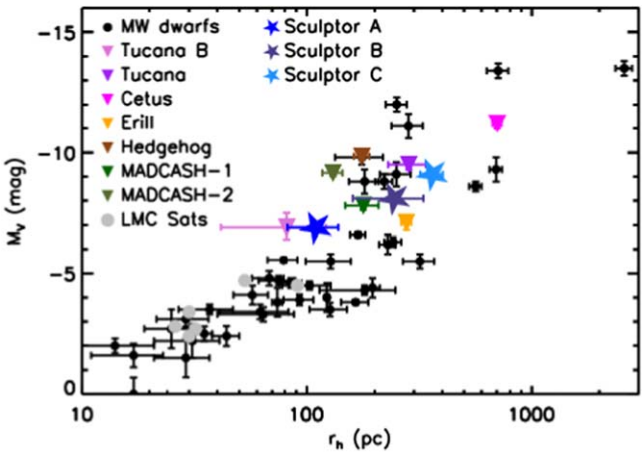

Figure 5. Absolute magnitude as a function of half-light radius of Sculptor A, B, and C. We also plot a variety of quenched dwarf galaxies in low-density environments. These include quenched dwarfs in the outskirts of the Local Group (Cetus: A. W. McConnachie & M. J. Irwin 2006; Tucana: I. Saviane et al. 1996; Eri II: D. Crnojević et al. 2016a; J. D. Simon et al. 2021); in isolated environments (Tucana B: D. J. Sand et al. 2022; Hedgehog: J. Li et al. 2024); around Magellanic Cloud analogs (MADCASH-1 and 2; J. L. Carlin et al. 2021); and the LMC itself (Reticulum II: B. Mutlu-Pakdil et al. 2018; Phoenix II: B. Mutlu-Pakdil et al. 2018; Horologium I: H. Richstein et al. 2024; Carina II: G. Torrealba et al. 2018; Carina III: G. Torrealba et al. 2018, Hydrus I: S. E. Koposov et al. 2018). Also plotted are the dwarf satellites of the Milky Way for context (see the Local Volume database: https://github.com/apace7/local_volume_database).

Sculptor A is most similar to Tucana B in several respects, including the fact that they are the only two isolated, quenched ultrafaint dwarf galaxies known. Both systems are

≈1.4 Mpc from the Milky Way ($\gtrsim$4.5 $r_{\rm vir,MW}$, assuming $r_{\rm vir,MW}$ = 200–300 kpc), likely too distant to be backsplash systems (e.g., M. Teyssier et al. 2012; T. Buck et al. 2019; E. Applebaum et al. 2021). They have very similar luminosities ($M_V = -6.9$; $L_V = 5 \times 10^4 L_\odot$) and sizes within the uncertainties. The two systems also share a lack of young stars and neutral hydrogen gas although this needs to be confirmed by deeper follow-up observations. Sculptor A, like Tucana B, likely has a low enough stellar mass to have been significantly affected by reionization and internal feedback in the early Universe ($M_* \lesssim 10^{5-6} M_\odot$; e.g., E. Applebaum et al. 2021).

Finally, Sculptor B ($M_V = -8.1$ mag) appears to be a brighter, more distant version of Sculptor A. It is somewhat fainter than the Milky Way satellites Draco ($M_V = -8.7$ mag; R. R. Muñoz et al. 2018) and Canes Venatici I ($M_V = -8.8$ mag; R. R. Muñoz et al. 2018) and significantly fainter than the Cetus and Tucana dwarfs, which are both suspected to be backsplash systems of the Milky Way. If Sculptor B is a distant backsplash system of NGC 300, it would be among the faintest examples of this class and provide a unique opportunity to study such systems around an LMC analog. If, however, it is unassociated with NGC 300, it is another candidate to be strongly affected by reionization or stellar feedback.

6. Conclusions and Implications

We have presented the discovery of three faint and ultrafaint dwarf galaxies in the direction of NGC 300, an isolated LMC analog. Deep Gemini GMOS follow-up imaging resolved each dwarf into stars, allowing us to determine their distance, luminosity, structure, and basic star formation properties. The dwarfs range in distance from ≈1.3 to 2.5 Mpc and have absolute magnitudes ranging from the ultrafaint regime (Sculptor A; $M_V = -6.9$ mag) to the faintest "classical" dwarfs ($M_V = -8.1$ and -9.1 mag for Sculptors B and C, respectively). All three dwarfs appear quenched, with an exclusively old stellar population, and no detectable H I gas reservoir or GALEX UV emission.

Interestingly, only one out of three of the dwarfs is clearly associated with NGC 300 itself, Sculptor C ($D = 2.04$ Mpc; $M_V = -9.1$ mag). The presence of Sculptor C is consistent with initial results from surveys searching for the faint satellite populations of Magellanic Cloud–analog systems (e.g., J. L. Carlin et al. 2016; J. L. Carlin et al. 2021; M. McNanna et al. 2024) although it is possible that the present search missed other dwarf galaxy candidates. In the near future, the DECam Local Volume Exploration Survey (A. Drlica-Wagner et al. 2021, 2022) will perform a systematic search for faint dwarf satellites around NGC 300 (and several other Magellanic Cloud–mass systems) in order to robustly constrain the population and compare it with expectations from cosmological simulations and the LMC itself.

Meanwhile, both Sculptor A and B are extremely faint, quenched dwarf galaxies in isolated environments ($\gtrsim$3.7 $r_{\rm vir,NGC300}$ and $\gtrsim$ 2.3$r_{\rm vir,NGC300}$ from NGC 300, respectively). It is possible that these systems are extreme backsplash systems (see discussion in I. M. E. Santos-Santos et al. 2023) and that their lack of gas and recent star formation is due to ram-pressure or tidal stripping during a close passage with a larger galaxy. Recent simulations have suggested that some backsplash systems may be evident out to ∼3–4 $r_{\rm vir}$ (e.g., J. A. Benavides et al. 2021) although similar simulations should be run for Magellanic Cloud–mass systems. To investigate this further, a velocity measurement of these dwarfs is necessary, along with further distance constraints.

If one or both of Sculptors A and B are not backsplash systems, then other mechanisms must be invoked to explain the lack of star formation and neutral gas. Isolated field dwarfs with $M_* > 10^7 M_\odot$ are almost all star-forming systems (M. Geha et al. 2012), but below this threshold, the quenched fraction is $\gtrsim$20% both in observations (C. T. Slater & E. F. Bell 2014) and simulations (e.g., C. R. Christensen et al. 2024). Without an interaction with a massive galaxy, Sculptor A or B may have been quenched by reionization and/or internal feedback (i.e., star formation or supernova feedback), which is seen in simulations of field dwarf galaxies (e.g., M. Jeon et al. 2017; M. P. Rey et al. 2020; E. Applebaum et al. 2021). Observations of the ultrafaint dwarfs of the Milky Way lend support to this picture (T. M. Brown et al. 2014; D. R. Weisz et al. 2014a; E. Sacchi et al. 2021; K. B. W. McQuinn et al. 2024) although the confounding effects of ram-pressure and tidal stripping complicate the interpretation. Confirming this picture for field dwarfs would be a strong verification of galaxy formation models at the lowest-mass scale.

Future H I, spectroscopic, and space-based data are needed to further understand the Sculptor dwarfs A, B, and C. A faint, extended gas reservoir, possibly offset from the optical emission, may signal the reaccretion of gas after reionization (e.g., M. P. Rey et al. 2022), and deep James Webb Space Telescope observations down to the oldest main-sequence turnoff would reveal the earliest epoch of star formation (e.g., D. Weisz & M. Boylan-Kolchin 2019). Bulk velocity information will shed light on the orbital and interaction history of the dwarfs as well.

Many more faint and ultrafaint dwarf galaxies are predicted at the edges of the Local Group and in nearby, low-density environments (E. J. Tollerud & J. E. G. Peek 2018), but initial efforts to find them have not always been successful (e.g., D. J. Sand et al. 2015b; E. J. Tollerud et al. 2015). Several upcoming programs such at Euclid (Euclid Collaboration et al. 2024), the Roman Space Telescope (R. Akeson et al. 2019), and the Rubin Observatory Legacy Survey of Space and Time (Z. Ivezić et al. 2019) are sure to find many more examples in the years ahead (e.g., M. K. Rodriguez Wimberly et al. 2019; B. Mutlu-Pakdil et al. 2021), which will provide demographic properties across environments.

Acknowledgments

Work on nearby galaxies by D.J.S. and the Arizona team acknowledges support from NSF grant AST-2205863. Research by D.C. is supported by NSF grant AST-1814208. K.S. acknowledges support from the Natural Sciences and Engineering Research Council of Canada (NSERC). J.E.A. and C.E.M-.V. are supported by the international Gemini Observatory, a program of NSF's NOIRLab, which is managed by the Association of Universities for Research in Astronomy (AURA) under a cooperative agreement with the National Science Foundation, on behalf of the Gemini partnership of Argentina, Brazil, Canada, Chile, the Republic of Korea, and the United States of America.

Based on observations obtained at the international Gemini Observatory under program GS-2022B-FT-103. Gemini Observatory is a program of NSF's NOIRLab, which is managed by the Association of Universities for Research in Astronomy (AURA) under a cooperative agreement with the National

Science Foundation on behalf of the Gemini Observatory partnership: the National Science Foundation (United States), National Research Council (Canada), Agencia Nacional de Investigación y Desarrollo (Chile), Ministerio de Ciencia, Tecnologìa e Innovación (Argentina), Ministério da Ciência, Tecnologia, Inovações e Comunicações (Brazil), and Korea Astronomy and Space Science Institute (Republic of Korea).

The work used images from the Dark Energy Camera Legacy Survey (DECaLS; Proposal ID 2014B-0404; PIs: David Schlegel and Arjun Dey). Full acknowledgment at https://www.legacysurvey.org/acknowledgment/.

This research is based on observations made with the Galaxy Evolution Explorer, obtained from the MAST data archive at the Space Telescope Science Institute, which is operated by the Association of Universities for Research in Astronomy, Inc., under NASA contract NAS 5-26555.

This work was performed in part at the Aspen Center for Physics, which is supported by National Science Foundation grant PHY-2210452.

Facilities: Gemini:South (GMOS), GALEX.

Software: astropy (Astropy Collaboration et al. 2013; The Astropy Collaboration et al. 2018), ASTROMETRY.NET (D. Lang et al. 2010) The IDL Astronomy User's Library (W. B. Landsman 1993), DAOPHOT (P. B. Stetson 1987, 1994), DRAGONS (K. Labrie et al. 2023a), (K. Labrie et al. 2023b, Version 3.1.0), SCAMP (E. Bertin 2006), SWARP (E. Bertin 2010).

ORCID iDs

David J. Sand https://orcid.org/0000-0003-4102-380X
Burçin Mutlu-Pakdil https://orcid.org/0000-0001-9649-4815
Michael G. Jones https://orcid.org/0000-0002-5434-4904
Ananthan Karunakaran https://orcid.org/0000-0001-8855-3635
Jennifer E. Andrews https://orcid.org/0000-0003-0123-0062
Paul Bennet https://orcid.org/0000-0001-8354-7279
Denija Crnojević https://orcid.org/0000-0002-1763-4128
Giuseppe Donatiello https://orcid.org/0000-0003-2536-5092
Alex Drlica-Wagner https://orcid.org/0000-0001-8251-933X
Catherine Fielder https://orcid.org/0000-0001-8245-779X
David Martínez-Delgado https://orcid.org/0000-0003-3835-2231
Clara E. Martínez-Vázquez https://orcid.org/0000-0002-9144-7726
Kristine Spekkens https://orcid.org/0000-0002-0956-7949
Amandine Doliva-Dolinsky https://orcid.org/0000-0001-9775-9029
Laura C. Hunter https://orcid.org/0000-0001-5368-3632
Jeffrey L. Carlin https://orcid.org/0000-0002-3936-9628
William Cerny https://orcid.org/0000-0003-1697-7062
Tehreem N. Hai https://orcid.org/0009-0005-9382-1362
Kristen B.W. McQuinn https://orcid.org/0000-0001-5538-2614
Andrew B. Pace https://orcid.org/0000-0002-6021-8760
Adam Smercina https://orcid.org/0000-0003-2599-7524

References

Abbott, T. M. C., Adamów, M., Aguena, M., et al. 2021, ApJS, 255, 20
Ahvazi, N., Benson, A., Sales, L. V., et al. 2024, MNRAS, 529, 3387
Akeson, R., Armus, L., Bachelet, E., et al. 2019, arXiv:1902.05569
Applebaum, E., Brooks, A. M., Christensen, C. R., et al. 2021, ApJ, 906, 96
Astropy Collaboration, Robitaille, T. P., Tollerud, E. J., et al. 2013, A&A, 558, A33
Barnes, D. G., Staveley-Smith, L., de Blok, W. J. G., et al. 2001, MNRAS, 322, 486
Battaglia, G., Taibi, S., Thomas, G. F., & Fritz, T. K. 2022, A&A, 657, A54
Benavides, J. A., Sales, L. V., Abadi, M. G., et al. 2021, NatAs, 5, 1255
Bennet, P., Sand, D. J., Crnojević, D., et al. 2019, ApJ, 885, 153
Bennet, P., Sand, D. J., Crnojević, D., et al. 2020, ApJL, 893, L9
Bennet, P., Sand, D. J., Crnojević, D., et al. 2022, ApJ, 924, 98
Benson, A. J., Frenk, C. S., Lacey, C. G., Baugh, C. M., & Cole, S. 2002, MNRAS, 333, 177
Bertin, E. 2006, in ASP Conf. Ser. 351, Astronomical Data Analysis Software and Systems XV, ed. C. Gabriel et al. (San Francisco, CA: ASP), 112
Bertin, E. 2010, SWarp: Resampling and Co-adding FITS Images Together, Astrophysics Source Code Library, ascl:1010.068
Bianchi, L., Shiao, B., & Thilker, D. 2017, ApJS, 230, 24
Brooks, A. M., Kuhlen, M., Zolotov, A., & Hooper, D. 2013, ApJ, 765, 22
Brown, T. M., Tumlinson, J., Geha, M., et al. 2014, ApJ, 796, 91
Buck, T., Macciò, A. V., Dutton, A. A., Obreja, A., & Frings, J. 2019, MNRAS, 483, 1314
Bullock, J. S., & Boylan-Kolchin, M. 2017, ARA&A, 55, 343
Bullock, J. S., Kravtsov, A. V., & Weinberg, D. H. 2000, ApJ, 539, 517
Cannon, J. M., Giovanelli, R., Haynes, M. P., et al. 2011, ApJL, 739, L22
Carlin, J. L., Mutlu-Pakdil, B., Crnojević, D., et al. 2021, ApJ, 909, 211
Carlin, J. L., Sand, D. J., Mutlu-Pakdil, B., et al. 2024, arXiv:2409.17437
Carlin, J. L., Sand, D. J., Price, P., et al. 2016, ApJL, 828, L5
Carlsten, S. G., Greene, J. E., Beaton, R. L., Danieli, S., & Greco, J. P. 2022, ApJ, 933, 47
Casey, K. J., Greco, J. P., Peter, A. H. G., & Davis, A. B. 2023, MNRAS, 520, 4715
Cerny, W., Martìnez-Vázquez, C. E., Drlica-Wagner, A., et al. 2023, ApJ, 953, L21
Chiboucas, K., Jacobs, B. A., Tully, R. B., & Karachentsev, I. D. 2013, AJ, 146, 126
Christensen, C. R., Brooks, A. M., Munshi, F., et al. 2024, ApJ, 961, 236
Crnojević, D., Sand, D. J., Bennet, P., et al. 2019, ApJ, 872, 80
Crnojević, D., Sand, D. J., Spekkens, K., et al. 2016b, ApJ, 823, 19
Crnojević, D., Sand, D. J., Zaritsky, D., et al. 2016a, ApJL, 824, L14
Dalcanton, J. J., Williams, B. F., Seth, A. C., et al. 2009, ApJS, 183, 67
Davis, A. B., Garling, C. T., Nierenberg, A. M., et al. 2024, arXiv:2409.03999
Dekel, A., & Silk, J. 1986, ApJ, 303, 39
Dey, A., Schlegel, D. J., Lang, D., et al. 2019, AJ, 157, 168
Diemer, B., & Kravtsov, A. V. 2015, ApJ, 799, 108
Doliva-Dolinsky, A., Martin, N. F., Thomas, G. F., et al. 2022, ApJ, 933, 135
Doliva-Dolinsky, A., Martin, N. F., Yuan, Z., et al. 2023, ApJ, 952, 72
Dotter, A., Chaboyer, B., Jevremović, D., et al. 2008, ApJS, 178, 89
Drlica-Wagner, A., Bechtol, K., Mau, S., et al. 2020, ApJ, 893, 47
Drlica-Wagner, A., Carlin, J. L., Nidever, D. L., et al. 2021, ApJS, 256, 2
Drlica-Wagner, A., Ferguson, P. S., Adamów, M., et al. 2022, ApJS, 261, 38
El-Badry, K., Quataert, E., Wetzel, A., et al. 2018, MNRAS, 473, 1930
Engler, C., Pillepich, A., Pasquali, A., et al. 2021, MNRAS, 507, 4211
Euclid Collaboration, Mellier, Y., Abdurro'uf, et al. 2024, arXiv:2405.13491
Garling, C. T., Peter, A. H. G., Spekkens, K., et al. 2024, MNRAS, 528, 365
Gatto, M., Bellazzini, M., Tortora, C., et al. 2024, A&A, 681, L13
Geha, M., Blanton, M. R., Yan, R., & Tinker, J. L. 2012, ApJ, 757, 85
Giovanelli, R., Haynes, M. P., Adams, E. A. K., et al. 2013, AJ, 146, 15
Hargis, J. R., Albers, S., Crnojević, D., et al. 2020, ApJ, 888, 31
Homma, D., Chiba, M., Komiyama, Y., et al. 2024, PASJ, 76, 733
Hook, I. M., Jørgensen, I., Allington-Smith, J. R., et al. 2004, PASP, 116, 425
Hopkins, P. F., Quataert, E., & Murray, N. 2012, MNRAS, 421, 3522
Iglesias-Páramo, J., Buat, V., Takeuchi, T. T., et al. 2006, ApJS, 164, 38
Into, T., & Portinari, L. 2013, MNRAS, 430, 2715
Ivezić, Z., Kahn, S. M., Tyson, J. A., et al. 2019, ApJ, 873, 111
Jeon, M., Besla, G., & Bromm, V. 2017, ApJ, 848, 85
Jones, M. G., Mutlu-Pakdil, B., Sand, D. J., et al. 2023, ApJL, 957, L5
Jones, M. G., Sand, D. J., Mutlu-Pakdil, B., et al. 2024, ApJL, 971, L37
Jordi, K., Grebel, E. K., & Ammon, K. 2006, A&A, 460, 339
Kalberla, P. M. W., & Haud, U. 2015, A&A, 578, A78
Kalberla, P. M. W., McClure-Griffiths, N. M., Pisano, D. J., et al. 2010, A&A, 521, A17
Karachentsev, I. D., & Kaisina, E. I. 2019, AstBu, 74, 111
Karachentsev, I. D., Karachentseva, V. E., Huchtmeier, W. K., & Makarov, D. I. 2004, AJ, 127, 2031
Karunakaran, A., Spekkens, K., Oman, K. A., et al. 2021, ApJL, 916, L19
Koposov, S. E., Walker, M. G., Belokurov, V., et al. 2018, MNRAS, 479, 5343
Labrie, K., Simpson, C., Cardenes, R., et al. 2023a, RNAAS, 7, 214
Labrie, K., Simpson, C., Turner, J., et al. 2023b, DRAGONS, v3.1.0, Zenodo, doi:10.5281/zenodo.7776065
Landsman, W. B. 1993, in ASP Conf. Ser. 52, Astronomical Data Analysis Software and Systems II, ed. R. J. Hanisch, R. J. V. Brissenden, & J. Barnes (San Francisco, CA: ASP), 246

Lang, D., Hogg, D. W., Mierle, K., Blanton, M., & Roweis, S. 2010, AJ, 139, 1782
Lee, J. C., Gil de Paz, A., Kennicutt, R. C. J., et al. 2011, ApJS, 192, 6
Li, J., Greene, J. E., Carlsten, S. G., & Danieli, S. 2024, arXiv:2406.00101
Mac Low, M.-M., & Ferrara, A. 1999, ApJ, 513, 142
Manwadkar, V., & Kravtsov, A. V. 2022, MNRAS, 516, 3944
Mao, Y.-Y., Geha, M., Wechsler, R. H., et al. 2021, ApJ, 907, 85
Mao, Y.-Y., Geha, M., Wechsler, R. H., et al. 2024, ApJ, 976, 117
Martin, D. C., Fanson, J., Schiminovich, D., et al. 2005, ApJL, 619, L1
Martin, N. F., de Jong, J. T. A., & Rix, H.-W. 2008, ApJ, 684, 1075
Martin, N. F., Ibata, R. A., McConnachie, A. W., et al. 2013, ApJ, 776, 80
McClure-Griffiths, N. M., Pisano, D. J., Calabretta, M. R., et al. 2009, ApJS, 181, 398
McConnachie, A. W. 2012, AJ, 144, 4
McConnachie, A. W., & Irwin, M. J. 2006, MNRAS, 365, 1263
McNanna, M., Bechtol, K., Mau, S., et al. 2024, ApJ, 961, 126
McQuinn, K. B. W., Cannon, J. M., Dolphin, A. E., et al. 2014, ApJ, 785, 3
McQuinn, K. B. W., Mao, Y.-Y., Buckley, M. R., et al. 2023, ApJ, 944, 14
McQuinn, K. B. W., Mao, Y.-Y., Tollerud, E. J., et al. 2024, ApJ, 967, 161
McQuinn, K. B. W., Skillman, E. D., Dolphin, A., et al. 2015, ApJ, 812, 158
McQuinn, K. B. W., Telidevara, A. K., Fuson, J., et al. 2021, ApJ, 918, 23
Moster, B. P., Somerville, R. S., Maulbetsch, C., et al. 2010, ApJ, 710, 903
Muñoz, R. R., Côté, P., Santana, F. A., et al. 2018, ApJ, 860, 66
Muñoz, J. C., Sheth, K., Regan, M., et al. 2015, ApJS, 219, 3
Mutlu-Pakdil, B., Sand, D. J., Carlin, J. L., et al. 2018, ApJ, 863, 25
Mutlu-Pakdil, B., Sand, D. J., Crnojević, D., et al. 2021, ApJ, 918, 88
Mutlu-Pakdil, B., Sand, D. J., Crnojević, D., et al. 2024, arXiv:2401.14457
Putman, M. E., Zheng, Y., Price-Whelan, A. M., et al. 2021, ApJ, 913, 53
Rey, M. P., Pontzen, A., Agertz, O., et al. 2020, MNRAS, 497, 1508
Rey, M. P., Pontzen, A., Agertz, O., et al. 2022, MNRAS, 511, 5672
Richstein, H., Kallivayalil, N., Simon, J. D., et al. 2024, ApJ, 967, 72
Ricotti, M., & Gnedin, N. Y. 2005, ApJ, 629, 259
Rodriguez Wimberly, M. K., Cooper, M. C., Fillingham, S. P., et al. 2019, MNRAS, 483, 4031
Sacchi, E., Richstein, H., Kallivayalil, N., et al. 2021, ApJL, 920, L19
Sales, L. V., Wetzel, A., & Fattahi, A. 2022, NatAs, 6, 897
Samuel, J., Wetzel, A., Chapman, S., et al. 2021, MNRAS, 504, 1379
Sand, D. J., Crnojević, D., Bennet, P., et al. 2015b, ApJ, 806, 95
Sand, D. J., Crnojević, D., Strader, J., et al. 2014, ApJL, 793, L7
Sand, D. J., Olszewski, E. W., Willman, B., et al. 2009, ApJ, 704, 898
Sand, D. J., Spekkens, K., Crnojević, D., et al. 2015a, ApJL, 812, L13
Sand, D. J., Strader, J., Willman, B., et al. 2012, ApJ, 756, 79
Sand, D. J., Mutlu-Pakdil, B., Jones, M. G., et al. 2022, ApJL, 935, L17
Santos-Santos, I. M. E., Navarro, J. F., & McConnachie, A. 2023, MNRAS, 520, 55
Saviane, I., Held, E. V., & Piotto, G. 1996, A&A, 315, 40
Sawala, T., Frenk, C. S., Fattahi, A., et al. 2016, MNRAS, 457, 1931
Schlafly, E. F., & Finkbeiner, D. P. 2011, ApJ, 737, 103
Simon, J. D. 2019, ARA&A, 57, 375
Simon, J. D., Brown, T. M., Drlica-Wagner, A., et al. 2021, ApJ, 908, 18
Slater, C. T., & Bell, E. F. 2014, ApJ, 792, 141
Smercina, A., Bell, E. F., Price, P. A., et al. 2018, ApJ, 863, 152
Smith, S. E. T., Cerny, W., Hayes, C. R., et al. 2024, ApJ, 961, 92
Smith, S. E. T., Jensen, J., Roediger, J., et al. 2023, AJ, 166, 76
Stetson, P. B. 1987, PASP, 99, 191
Stetson, P. B. 1994, PASP, 106, 250
Teyssier, M., Johnston, K. V., & Kuhlen, M. 2012, MNRAS, 426, 1808
The Astropy Collaboration, Price-Whelan, A. M., & Sipöcz, B. M. 2018, AJ, 156, 123
Tollerud, E. J., Geha, M. C., Grcevich, J., Putman, M. E., & Stern, D. 2015, ApJL, 798, L21
Tollerud, E. J., & Peek, J. E. G. 2018, ApJ, 857, 45
Torrealba, G., Belokurov, V., Koposov, S. E., et al. 2018, MNRAS, 475, 5085
van der Marel, R. P., Alves, D. R., Hardy, E., Suntzeff, N. B., et al. 2002, AJ, 124, 2639
Walsh, S. M., Willman, B., Sand, D., et al. 2008, ApJ, 688, 245
Weerasooriya, S., Bovill, M. S., Benson, A., Musick, A. M., & Ricotti, M. 2023, ApJ, 948, 87
Weisz, D., & Boylan-Kolchin, M. 2019, BAAS, 51, 1
Weisz, D. R., Dalcanton, J. J., Williams, B. F., et al. 2011, ApJ, 739, 5
Weisz, D. R., Dolphin, A. E., Skillman, E. D., et al. 2014a, ApJ, 789, 147
Weisz, D. R., Skillman, E. D., Hidalgo, S. L., et al. 2014b, ApJ, 789, 24
Wetzel, A. R., Hopkins, P. F., Kim, J.-h., et al. 2016, ApJL, 827, L23